analytical chemistry

pubs.acs.org/ac Article

Regulation of Target-activated CRISPR/Cas12a on Surface Binding of Polymer Dots for Sensitive Electrochemiluminescence DNA Analysis

Lele Li, Siqi Yu, Jie Wu, and Huangxian Ju*

Cite This: *Anal. Chem.* 2023, 95, 7396−7402 Read Online

ACCESS | Metrics & More | Article Recommendations | Supporting Information

ABSTRACT: Polymer dots (Pdots) have emerged as a type of attractive electrochemiluminescence (ECL) emitter. However, the low ECL efficiency severely limits their practicability. In this work, we develop a sensitive ECL biosensing strategy for the detection of human papilloma virus subtype (HPV-16) DNA by using target-activated CRISPR/Cas12a to regulate the binding of Pdots-DNA to biosensor and local surface plasmon resonance (LSPR) effect of electrochemically deposited Au nanoparticles (depAuNPs) to enhance the ECL emission of Pdots bound on biosensor. The biosensor is prepared by simply assembling hairpin DNA on depAuNPs modified electrode. In the presence of target DNA, the designed specific CRISPR/Cas12a can be activated to digest single-stranded assistant DNA, which decreases the amount of hairpin DNA opened by assistant DNA to bind Pdots-DNA on the biosensor surface, thus reduces the ECL emission. The integration of target DNA-triggered catalysis and the LSPR effect of depAuNPs greatly improves the sensitivity of ECL analysis. Using HPV-16 DNA as a target model, the proposed method shows a limit of detection (LOD) of 3.2 fM at a signal-to-noise ratio of 3 and a detectable concentration range of 5.0 fM to 50 pM. The high sensitivity, excellent selectivity, good testing stability, and acceptable fabrication reproducibility of the designed ECL biosensing strategy demonstrate its potential application in DNA bioanalysis.

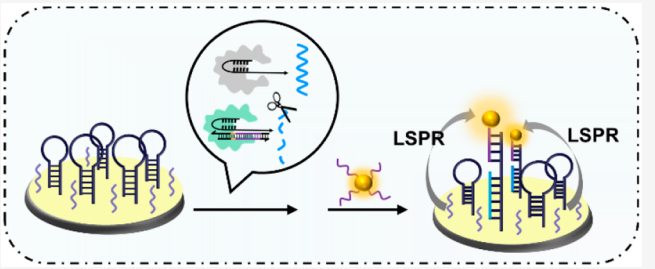

INTRODUCTION

Electrochemiluminescence (ECL) is an electrochemically triggered luminescence technology, integrating the advantages of electrochemistry and chemiluminescence.[1] The use of electric potential rather than an external light as the excitation source leads to low background signal, electrochemical controllability, high sensitivity, and simple operation.[2−4] ECL luminophores play the most important role in the ECL process. However, traditional luminescent materials are often faced with the problems of high biological toxicity, difficult modification, a complex functional modification process, and high cost, which to a large extent limit their application.[5−7] Therefore, the constant search for new ECL luminescent materials is a long-term topic of this field. As a type of emerging ECL emitters, organic polymer dots (Pdots) are mainly composed of π-conjugated polymers with a particle size of 20−30 nm.[8,9] Due to their good biocompatibility, nontoxicity, easy functionalization, high photostability, and tunable luminescence, Pdots have been rapidly developed and applied in biological and chemical analysis.[10−12] For example, our previous work utilized silole-containing Pdots as ECL emitters to achieve sensitive detection of dopamine.[13] Currently, the key challenge for Pdots is their relatively lower ECL efficiency than that of general inorganic emitters.[14] Accordingly, there is an urgent need to introduce signal amplification strategies for improving ECL performance of Pdots.

CRISPR (clustered regularly interspaced short palindromic repeats) system as a powerful gene editing tool has been considered as an excellent signal amplification strategy for the development of biosensing field.[15−17] This system consists of CRISPR-associated proteins (Cas) and related guide CRISPR RNA (crRNA).[18−20] Notably, the newly founded CRISPR/Cas12a trans-cleavage activity, namely, Cas12a and its corresponding CRISPR RNA (crRNA; Cas12a/crRNA duplex), can specifically recognize and cleavage specific DNA based on the recognition of protospacer adjacent motif (PAM) sequence,[21,22] which endows CRISPR/Cas12a with remarkable signal amplification ability and precise specificity.[23,24] A CRISPR/Cas12a-based ratiometric fluorescent sensor has been constructed by digesting TAMRA-labeled DNA with Burkholderia pseudomallei (Bp) DNA activated CRISPR/Cas12a for Bp DNA detection,[25] and human papilloma virus (HPV-16)-activated CRISPR/Cas12a has been used to increase the photocurrent of Nd-doped BiOBr nanosheets for sensitive detection of HPV-16.[26] The HPV-16 activated

Received: April 7, 2023
Accepted: April 21, 2023
Published: April 29, 2023

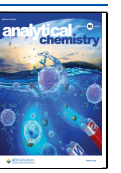

https://doi.org/10.1021/acs.analchem.3c01521
Anal. Chem. 2023, 95, 7396−7402

Scheme 1. Schematic Diagrams of (A) Pdots-DNA Preparation, (B) CRISPR Reaction Mixture, and (C) Biosensor Fabrication and ECL Detection of DNA

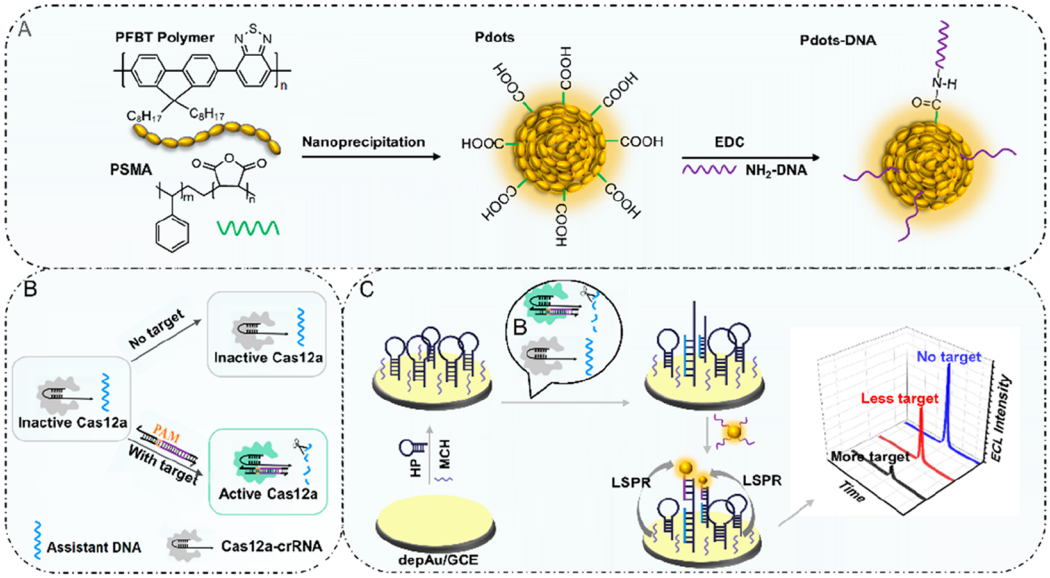

CRISPR/Cas12a has also been used to cleave off methylene blue (MB)-labeled ssDNA from electrode surface for electrochemical biosensing of HPV-16.[21] Using L-methionine stabilized gold nanoclusters (Met-AuNCs)[27] and [Ru(phen)$_2$dppz]$^{2+}$[28] as ECL emitters, two ECL methods have been developed for sensitive detection of DNA and microRNA. This work designed a CRISPR/Cas12a system along with a single-stranded assistant DNA for signal amplification. This system could be activated by the recognition of crRNA with target DNA to catalyze the digestion of assistant DNA. After dropping the digestion mixture on a hairpin DNA modified electrode, the undigested assistant DNA could open the hairpin DNA to bind Pdots-DNA, which achieved the regulation of surface binding of Pdots, and thus led to a novel ECL method for target DNA analysis (Scheme 1).

In order to further improve the sensitivity of the ECL method, a glassy carbon electrode deposited electrochemically with Au nanoparticles (depAu/GCE) was used for the assembly of hairpin DNA, which was inspired by the localized surface plasmon resonance (LSPR) effect of noble metals such as Au, Ag, and Pt.[29] The LSPR is a strong photon-driven coherent oscillation of surface-conducted electrons and occurs under appropriate light excitation on the surface of plasmonic materials.[30−32] This effect has been used to improve the biosensing performance for the detection of pancreatic cancer exosomes.[33] Here, human papilloma virus subtype (HPV-16) DNA, which is closely related to cervical cancer pathogenesis,[34,35] was used as a target model. The integration of target DNA-triggered catalysis and the strong LSPR effect of depAuNPs[36−38] greatly improved the sensitivity of the proposed ECL biosensing method for HPV-16 DNA. The high sensitivity along with a limit of detection (LOD) of 3.2 fM at a signal-to-noise ratio of 3, wide detectable concentration range, excellent selectivity, good testing stability, and acceptable fabrication reproducibility demonstrated the potential application of the designed ECL biosensing strategy in DNA bioanalysis.

EXPERIMENTAL SECTION

Materials, Reagents, and Apparatus. The detailed information is described in the Supporting Information (SI) and Table S1.

Preparation of PFBT Pdots and Pdots-DNA. PFBT Pdots were prepared in aqueous solution through nanoprecipitation.[39] In brief, 1 mg mL^{-1} of stock solutions of the PFBT copolymer and PSMA were prepared in THF to obtain a mixture of 50 μg mL^{-1} PFBT and 10 μg mL^{-1} PSMA. After ultrasonic degassing for 20 min, 1 mL of the mixture was quickly added to 4 mL of Milli-Q water in a vigorous bath sonicator (120 W, 37 kHz) for 4 min. THF was removed by rotary evaporation under vacuum and then filtered through a 0.22 μm poly(ether sulfones) (PES) syringe filter (Millex-GP Filter, Millipore) to obtain a carboxylated PFBT Pdots dispersion. The resulting PFBT Pdots dispersion was clear and stable for months without signs of aggregation.

The PFBT Pdots were functionalized with NH$_2$-DNA utilizing a typical EDC-catalyzed conjugation reaction between carboxylated Pdots and amine-containing DNA biomolecules.[40] For the conjugate reaction, the carboxylated Pdots dispersion (50 μg mL^{-1} in Milli-Q water, 3 mL), HEPES buffer (1 M, 60 μL), and polyethylene glycol (5% w/v PEG, Mw 3350, 60 μL) were completely mixed, and the pH was adjusted to 7.1 with 0.1 M NaOH. The presence of PEG could prevent nonspecific adsorption of biomolecules. The NH$_2$-DNA (100 μM, 60 μL) and freshly prepared EDC solution (5 mg mL^{-1} in Milli-Q water, 60 μL) were then added to the mixture and vibrated for 4 h at room temperature to obtain Pdots-DNA conjugates. The resulting Pdots-DNA was ultrafiltrated three times to remove free NH$_2$-DNA, and the purified Pdots-DNA was stored at 4 °C for further use.

Fabrication of Hairpin DNA Modified Electrode. A GCE was carefully polished with 0.05 μm alumina slurry and then sonicated in alternating ethanol and water. After drying with N$_2$, the cleaned GCE was immersed in HAuCl$_4$ solution (w/v = 1%) and in situ electrodeposited with gold nanoparticles for 30 s at a potential of −0.2 V to obtain depAu/GCE.[41]

https://doi.org/10.1021/acs.analchem.3c01521
Anal. Chem. 2023, 95, 7396−7402

Twenty μL of annealed hairpin DNA (10 μM) was mixed with 4 μL of TCEP (10 mM), incubated at room temperature for 1 h to reduce disulfide bonds, and then diluted with PBS to obtain 1 μM hairpin DNA.[42] Next, 10 μL of hairpin DNA was assembled on the depAu/GCE through Au−S bonds at 4 °C for 12 h. Afterward, 5 μL of MCH (1.0 mM) was immobilized on the electrode for 0.5 h to obtain the ECL biosensor and stored for later use.

Target-Activated CRISPR/Cas12a and ECL DNA Detection. HPV-16 DNA was annealed in 1× hybridization buffer (20 nM Tris-Cl, pH 7.5, 100 mM KCl, 5 mM $MgCl_2$) by heating at 95 °C for 5 min and slowly cooling to room temperature to prepare 1.0 μM of HPV-16 double-stranded DNA (HPV-16, dsDNA). Meanwhile, Cas12a was mixed with $crRNA_{HPV-16}$ in a 1:1.2 ratio in Cas buffer (10 mM Tris-HCl, 50 mM NaCl, 10 mM $MgCl_2$, 100 μg/mL BSA, pH 7.9) and incubated at 37 °C for 30 min to form a Cas12a-crRNA duplex. Then, 40 μL of 0.25 μM assistant DNA and 40 μL of HPV-16 dsDNA at different concentrations (0, 0.005, 0.01, 0.05, 0.1, 0.5, 1, 5, 10, and 50 pM) were added to 108 μL of Cas buffer to mix with 12 μL of the prepared Cas12a-crRNA duplex. Finally, the mixture was incubated at 37 °C for 60 min to activate Cas12a activity and digest assistant DNA, followed by incubation at 70 °C for 10 min to deactivate Cas12a and prevent the digestion reaction.[43]

Ten μL of the resulting digestion mixture was dropped on the ECL biosensor to incubate for 2 h at 37 °C, followed by the incubation of Pdots-DNA (10 μL) for 2 h. After each step, the biosensor was rinsed with RNase-free water to acquire an RNase-free environment for CRISPR/Cas system and dried with nitrogen. ECL measurements were performed in a 0.1 M PBS (pH 7.4) containing 0.1 M KNO_3 and 25 mM tri-n-propylamine (TPrA) with potential scanning from 0 to +1.4 V and a photomultiplier tube (PMT) at 600 V.

ECL Efficiency of PFBT Pdots. The relative ECL efficiency (Φ_{ECL}) of PFBT Pdots was evaluated with $Ru(bpy)_3^{2+}$ as a reference and the following equation:[44]

$$\Phi_{ECL} = \left(\frac{\int_0^t I\ dt}{\int_0^t i\ dt}\right)_x \Big/ \left(\frac{\int_0^t I\ dt}{\int_0^t i\ dt}\right)_{st} \quad (1)$$

where x and st represent ECL emitters, PFBT Pdots, and $[Ru(bpy)_3]^{2+}$, respectively. I and i represent the ECL intensity and current value, which were obtained by dropping 20 μL of 0.12 mg mL^{-1} PFBT Pdots or 1.0 mM $Ru(bpy)_3^{2+}$ on a pretreated GCE, and then immersing in 0.1 M PBS containing 25 mM TPrA as coreactant to scan the potential from 0 V to +1.6 V. The PMT was at 300 V.

Polyacrylamide Gel Electrophoresis (PAGE) Analysis. Four μL of DNA or reaction mixture, 1 μL of 6× loading buffer, and 1 μL of 6× UltraPower dye were prepared to perform 15% PAGE analysis by running at 90 V for 50 min. Bio-Rad ChemDoc XRS facility was used to obtain the resulting boards.

RESULTS AND DISCUSSION

Morphological and Optical Characteristics of PFBT Pdots. The PFBT Pdots were prepared by nanoprecipitation using PFBT polymer as luminescent precursor and PSMA as carboxyl functionalized copolymer. After hydrolysis by maleic anhydride, a large number of carboxyl groups were generated on the surface of PFBT Pdots (Scheme 1A). The morphology

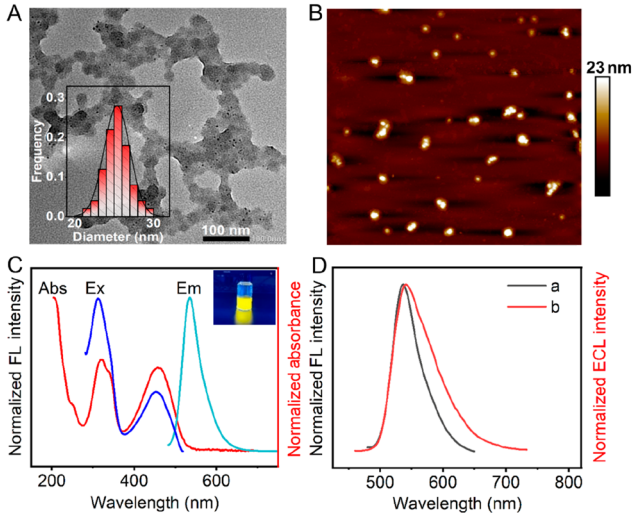

Figure 1. (A) TEM and (B) AFM images of PFBT Pdots. Inset in (A): size distribution of Pdots. (C) Fluorescence and UV−vis absorption spectra of PFBT Pdots dispersed in water. Inset: photograph of Pdots solution illuminated at 365 nm. (D) Fluorescence spectrum of PFBT Pdots (curve a) and ECL spectrum of PFBT Pdots modified GCE (curve b) in 0.1 M PBS with 25 mM TPrA.

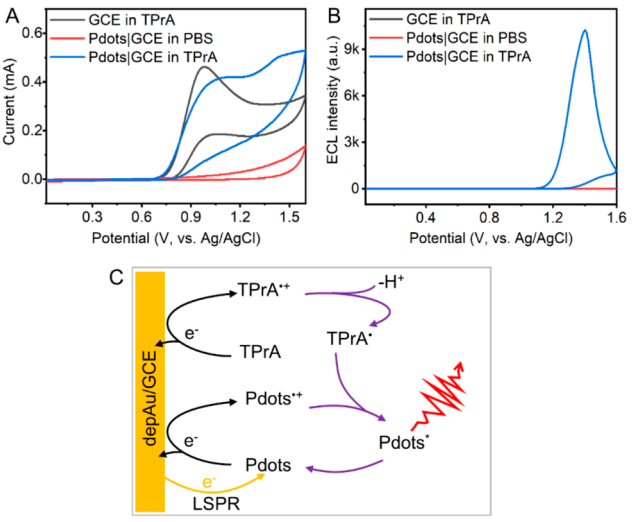

Figure 2. (A) CV and (B) ECL-potential curves of bare and PFBT Pdots modified GCE in 0.1 M pH 7.4 PBS in absence and presence of 25 mM TPrA. (C) ECL mechanism of PFBT Pdots modified depAu/GCE with TPrA as coreactant.

of the prepared PFBT Pdots was characterized by transmission electron microscopy (TEM) and atomic force microscopy (AFM). The results showed the spherical and monodisperse feature of PFBT Pdots with diameters distribution ranging from 20 to 30 nm (Figure 1A) and a height of 23 nm (Figures 1B and S1).

The optical properties of PFBT Pdots were investigated by UV−vis absorption, fluorescence (FL), and ECL spectra. The UV−vis absorption spectrum showed three characteristic absorption peaks of PFBT Pdots at 249, 323, and 460 nm (Figure 1C). The Pdots could be illuminated at 365 nm, and showed the maximum FL emission at 535 nm at an optimal excitation wavelength of 323 nm (Figure 1C). The ECL

https://doi.org/10.1021/acs.analchem.3c01521
Anal. Chem. 2023, 95, 7396−7402

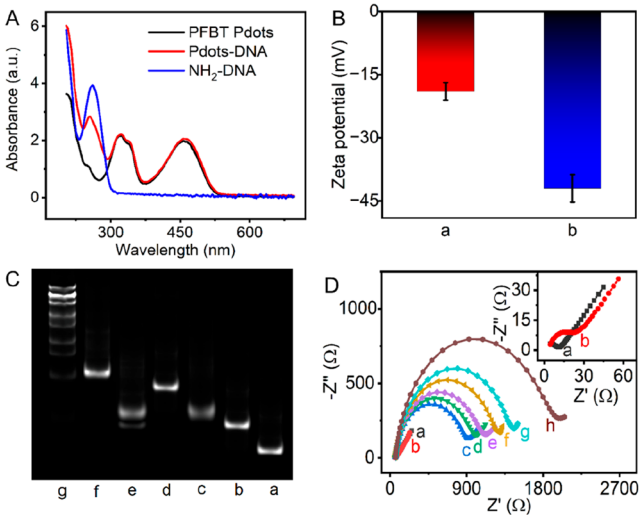

Figure 3. (A) UV−vis spectra of PFBT Pdots, Pdots-DNA, and NH_2-DNA. (B) Zeta potentials of PFBT Pdots (a) and Pdots-DNA (b). (C) PAGE images for 2 μM assistant DNA (a), NH_2-DNA (b), hairpin DNA (c), (c) + (a) (d), (c) + (b) (e), (c) + (a) + (b) (f), and 15−300 bp markers (g) in Tris-HCl buffer (pH 7.4). (D) EIS of bare GCE (a), depAu/GCE (b), HP/depAu/GCE (c), MCH/HP/depAu/GCE (d), MCH/HP/depAu/GCE in presence (e) and absence (f) of target-activated CRISPR/Cas12a mixture, (e) +Pdots-DNA (g), and (f) +Pdots-DNA (h).

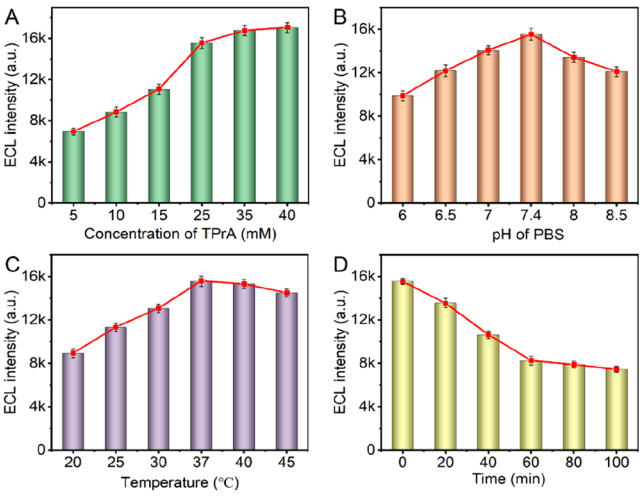

Figure 4. Optimization of (A) TPrA concentration, (B) pH of PBS, (C) target-activated digestion temperature, and (D) digestion time for ECL detection of HPV16 DNA (n = 3).

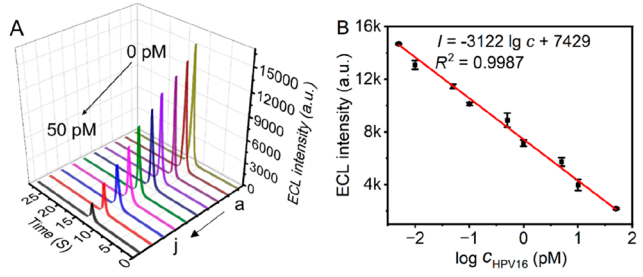

Figure 5. (A) ECL-time curves of ECL biosensor at 0, 0.005, 0.01, 0.05, 0.1, 0.5, 1, 5, 10, and 50 pM HPV-16 (from a to j). (B) Calibration curve for HPV-16 detection (n = 3).

emission peak of PFBT Pdots occurred at the same wavelength as that of the fluorescence spectrum (Figure 1D), indicating that the ECL was generated by the bandgap emission of PFBT Pots.[45] The ECL efficiency of PFBT Pdots relative to commercial $[Ru(bpy)_3]^{2+}$ was evaluated to be 39.3% (vs 1 mM $[Ru(bpy)_3]^{2+}$/TPrA, Table S2). The relatively high ECL efficiency resulted from the large conjugated structure of Pdots, which was also an advantage of conjugated Pdots over other inorganic and small-molecular ECL emitters.

ECL Mechanism. At GCE, TPrA showed an irreversible oxidation peak at +0.98 V with an onset potential of +0.57 V.[46] The oxidation peak potential was slightly more positive at PFBT Pdots modified GCE (Pdots|GCE) (Figure 2A), and could be attributed to the oxidation of TPrA to form $TPrA^{\bullet+}$. In the same potential range, the Pdots|GCE showed relatively weak oxidation wave, which could also be observed in the presence of TPrA, suggesting that Pdots could be electrochemically oxidized to form cationic radicals by injecting holes into the highest occupied molecular orbital.[47]

Both TPrA and Pdots|GCE did not show any ECL emission in PBS, while a strong ECL emission of Pdots|GCE was observed at +1.4 V when the detection solution PBS contained TPrA (Figure. 2B), which suggested that TPrA could act as a coreactant of PFBT Pdots to generate a stable ECL signal through the reaction of hole injected Pdots with electrooxidation and then deprotonation formed $TPrA^{\bullet}$ to generate excited Pdots*.[48] The relevant reaction formulas were described as follows:

$$TPrA - e^- \rightarrow TPrA^{\bullet+} \quad (2)$$

$$TPrA^{\bullet+} - H^+ \rightarrow TPrA^{\bullet} \quad (3)$$

$$Pdots - e^- \rightarrow Pdots^{\bullet+} \quad (4)$$

$$TPrA^{\bullet} + Pdots^{\bullet+} \rightarrow Pdots^* + TPrA_{ox} \quad (5)$$

$$Pdots^* \rightarrow Pdots + h\nu \quad (6)$$

At the electrochemically deposited AuNPs modified electrode, the LSPR effect could enhance the ECL emission of Pdots (Figure S2) through a strong photon-driven coherent oscillation of surface-conducted electrons under light excitation.[33] The AuNPs scattered the incident light and further locally amplified the electric field from the light generated by the ECL reaction of Pdots, thus transferring LSPR excited electrons to the Pdots to promote the formation of $Pdots^{*+}$ on the biosensor surface (Figure 2C).

Characterization and Binding Feasibility of Pdots-DNA. After PFBT Pdots were functionalized with NH_2-DNA, the Pdots-DNA showed three absorption peaks at 255, 323, and 460 nm (Figure 3A). The absorption peaks at 323 and 460 nm were consistent with those of PFBT Pdots, while the absorption peak at 255 nm was the merge of PFBT Pdots absorption at 249 nm with NH_2-DNA absorption at 261 nm, and much stronger than that of PFBT Pdots, indicating that NH_2-DNA was successfully conjugated to the surface of Pdots. The conjugation resulted in increasing zeta-potential from −19 mV of Pdots to −42 mV of Pdots-DNA (Figure 3B).

Polyacrylamide gel electrophoresis (PAGE) was used to verify the feasibility of assistant DNA triggered binding of Pdots-DNA. As shown in Figure 3C, the hybridization of hairpin DNA (lane c) with assistant DNA (lane a) produced a band at larger molecular weight (lane d), which further increased after NH_2-DNA (lane b) was added in the mixture of

https://doi.org/10.1021/acs.analchem.3c01521
Anal. Chem. 2023, 95, 7396−7402

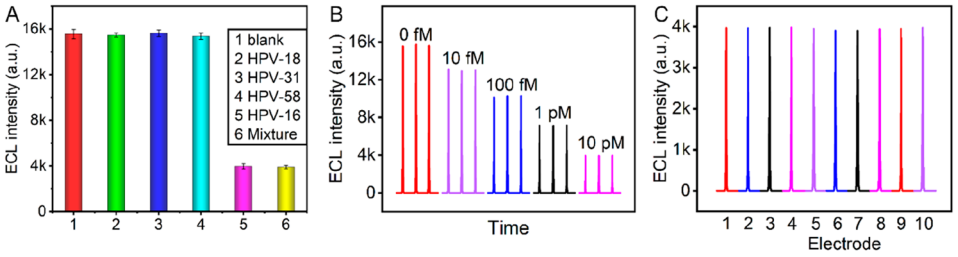

Figure 6. (A) Specificity of the biosensing method tested with blank (PBS), 1 nM HPV-18, 1 nM HPV-31, 1 nM HPV-58, 10 pM HPV-16, and the mixture of 10 pM HPV-16, 1 nM HPV-18, HPV-31 and HPV-58 (n = 3). (B) Testing stability of the biosensors scanned for 3 consecutive cycles at different HPV-16 concentration. (C) Reproducibility of ten ECL biosensors at 10 pM HPV-16. ECL measurements were performed in 0.1 M PBS (pH 7.4) containing 25 mM TPrA.

hairpin DNA and assistant DNA (lane f), indicating the hybridization of NH_2-DNA with the hairpin DNA after it was opened by assistant DNA (Figure S3). Moreover, the mixture of hairpin DNA and NH_2-DNA did not show their hybridization (lane e), indicating the feasibility of using assistant DNA to regulate the binding of NH_2-DNA with hairpin DNA. The regulation could be performed on the biosensor surface for the binding of Pdots-DNA.

Electrochemical impedance spectroscopic (EIS) measurements were performed to characterize the assembly process for biosensor fabrication and surface Pdots-DNA binding (Figure 3D). Both bare GCE and depAu/GCE showed negligible electron-transfer resistance (R_{et}; <30 Ω, curves a and b). The R_{et} value increased accordingly with the self-assembly of negatively charged hairpin DNA (HP) (curve c) and sealing of nonconductive MCH (curve d). It continued to increase with successive incubation of target-activated (curve e) or no-target CRISPR mixture (curve f) on the electrode, indicating that more amount of assistant DNA in no-target CRISPR mixture was bound to HP modified depAu/GCE to open the HP, which resulted in the binding of more Pdots-DNA on the biosensor surface. Thus, no-target CRISPR mixture incubated HP/depAu/GCE showed larger R_{et} value than target-activated CRISPR mixture incubated HP/depAu/GCE (curves g and h), in which a part of the assistant DNA was digested by activated CRISPR/Cas12a, demonstrating the feasibility of the biosensing strategy for target DNA detection.

Optimization of Target-Activated Digestion and ECL Detection Conditions. As an ECL coreactant of PFBT Pdots, TPrA concentration was an important factor affecting the detection performance. The ECL intensity increased with increasing TPrA concentration and reached a plateau value at 25 mM, which was chosen for ECL detection of the target DNA. In order to achieve high sensitivity, the pH of ECL detection solution, and target-activated digestion temperature and time were also optimized. With the increasing pH of 0.1 M PBS the ECL intensity increased and reached a maximum at pH 7.4 (Figure 4B). Thus, pH 7.4 0.1 M PBS containing 0.1 M KNO_3 and 25 mM TPrA was used for ECL detection. Similarly, optimal target-activated digestion temperature and time were 37 °C (Figure 4C) and 60 min (Figure 4D).

ECL Biosensing Performance for HPV-16 Detection. Under optimal conditions, the Pdots-DNA was introduced onto the electrode surface for ECL measurements. As the concentration of HPV-16 increased from 5.0 fM to 50 pM, the ECL intensity decreased (Figure 5A). The ECL intensity (I) depended linearly on the logarithm of HPV-16 concentration with a linear equation of $I = -3122 \lg c + 7429$ (R^2 = 0.9987) and a limit of detection (LOD) of 3.2 fM at a signal-to-noise ratio of 3 (Figure 5B). Compared with several electrochemical biosensors previously reported for HPV-16 detection, the proposed ECL biosensor showed a wider detection range and a lower LOD (Table S3). Moreover, the CRISPR/Cas12a regulating strategy also showed better performance than rolling circle amplification-assistant Pdots-based ECL biosensor for DNA (Table S4).

The selectivity of the biosensor was evaluated by comparing the ECL responses of DNA interferents with different sequences, including HPV-18, HPV-31 and HPV-58, and HPV-16 (target). The concentration of each interfering sequence (1 nM) was 100 times higher than that of target HPV-16 (10 pM). As expected, these interferents showed the same signal as that of the blank, while the mixture of HPV-18, HPV-31, HPV-58, and HPV-16 showed the same response as that of HPV-16 (Figure 6A), indicating the negligible effect of these interferents on target detection, and thus the excellent selectivity of the biosensing strategy.

After incubating the DNA biosensors with target-activated digestion mixtures obtained at different target concentrations and then Pdots-DNA, these biosensors showed stable ECL responses with the continuous ECL measurements (Figure 6B), indicating good testing stability and ECL detection accuracy. The fabrication reproducibility of the biosensors was examined by measuring ECL signal of 100 fM HPV-16 DNA with 10 independent electrodes. The results showed acceptable reproducibility with a relative standard deviation (RSD) of 3.2% (Figure 6C).

Real Samples Analysis. Clinical sample of cervical cancer patients was obtained from Jiangsu Province Hospital (Jiangsu, China). The concentration of HPV-16 DNA in this sample was detected with the proposed method to be 492 fM. To verify the accuracy of this result, different concentrations of HPV-16 DNA (10, 100, 500 fM, and 1.0 pM) were added in this sample for recovery test, respectively. The results showed that the recoveries ranged from 96.0% to 103.8% and the RSD ranged from 2.87% to 4.23% (Table S5), indicating good accuracy and that the proposed biosensor possessed promising prospect in DNA analysis of clinical samples.

CONCLUSION

This work has developed a sensitive ECL biosensing strategy for DNA analysis by integrating target DNA-triggered CRISPR/Cas12a catalysis and the LSPR effect of depAuNPs to enhance the ECL response of bound Pdots-DNA. The relativity of ECL response with target concentration is constructed by the CRISPR/Cas12a catalyzed digestion of assistant DNA to regulate the binding of Pdots-DNA on

https://doi.org/10.1021/acs.analchem.3c01521
Anal. Chem. 2023, 95, 7396−7402

biosensor surface, which can be performed with a hairpin DNA modified electrode. The proposed DNA biosensing strategy achieves sensitive quantification of target HPV-16 DNA with high sensitivity, excellent selectivity, good accuracy and acceptable fabrication reproducibility. Therefore, it possesses potential application in DNA bioanalysis.

■ ASSOCIATED CONTENT

Supporting Information

The Supporting Information is available free of charge at https://pubs.acs.org/doi/10.1021/acs.analchem.3c01521.

Materials, reagents, and apparatus, AFM images of PFBT Pdots, schematic diagrams of surface binding of PFBT Pdots, oligonucleotide sequences, ECL efficiency of PFBT Pdots, performance comparison of biosensors for HPV-16, comparison of Pdots-based ECL biosensors for DNA, and sample analysis (PDF)

■ AUTHOR INFORMATION

Corresponding Author

Huangxian Ju − *State Key Laboratory of Analytical Chemistry for Life Science, School of Chemistry and Chemical Engineering, Nanjing University, Nanjing 210023, People's Republic of China;* orcid.org/0000-0002-6741-5302; Phone: +86-25-89683593; Email: hxju@nju.edu.cn

Authors

Lele Li − *State Key Laboratory of Analytical Chemistry for Life Science, School of Chemistry and Chemical Engineering, Nanjing University, Nanjing 210023, People's Republic of China*

Siqi Yu − *State Key Laboratory of Analytical Chemistry for Life Science, School of Chemistry and Chemical Engineering, Nanjing University, Nanjing 210023, People's Republic of China*

Jie Wu − *State Key Laboratory of Analytical Chemistry for Life Science, School of Chemistry and Chemical Engineering, Nanjing University, Nanjing 210023, People's Republic of China;* orcid.org/0000-0003-1379-122X

Complete contact information is available at: https://pubs.acs.org/10.1021/acs.analchem.3c01521

Notes

The authors declare no competing financial interest.

■ ACKNOWLEDGMENTS

We acknowledge the financial support of the National Natural Science Foundation of China (21890741, 21827812), the Science and Technology Project of Nanjing City (202110023), and the Canon Medical Systems Corporation (2022200494).

■ REFERENCES

(1) Chen, M. M.; Cheng, S. B.; Ji, K.; Gao, J.; Liu, Y. L.; Wen, W.; Zhang, X.; Wang, S.; Huang, W. H. *Chem. Sci.* **2019**, *10*, 6295−6303.

(2) Wang, N. N.; Gao, H.; Li, Y. Z.; Li, G. M.; Chen, W. W.; Jin, Z. C.; Lei, J. P.; Wei, Q.; Ju, H. X. *Angew. Chem., Int. Ed.* **2021**, *60*, 197−201.

(3) Gu, W. L.; Wang, H. J.; Jiao, L.; Wu, Y.; Chen, Y. X.; Hu, L. Y.; Gong, J. M.; Du, D.; Zhu, C. Z. *Angew. Chem., Int. Ed.* **2020**, *59*, 3534−3538.

(4) Wang, N. N.; Feng, Y. Q.; Wang, Y. W.; Ju, H. X.; Yan, F. *Anal. Chem.* **2018**, *90*, 7708−7714.

(5) Wang, N. N.; Chen, L. Z.; Chen, W. W.; Ju, H. X. *Anal. Chem.* **2021**, *93*, 5327−5333.

(6) Dong, Y. P.; Wang, J.; Peng, Y.; Zhu, J. J. *Biosens. Bioelectron.* **2017**, *89*, 1053−1058.

(7) Xia, H. Y.; Zheng, X. L.; Li, J.; Wang, L. G.; Xue, Y.; Peng, C.; Han, Y. C.; Wang, Y.; Guo, S. J.; Wang, J.; Wang, E. *J. Am. Chem. Soc.* **2022**, *144*, 7741−7749.

(8) Wu, C. F.; Chiu, D. T. *Angew. Chem., Int. Ed.* **2013**, *52*, 3086−3109.

(9) Zhang, B. Y.; Wang, F.; Zhou, H.; Gao, D. Y.; Yuan, Z.; Wu, C. F.; Zhang, X. J. *Angew. Chem., Int. Ed.* **2019**, *58*, 2744−2748.

(10) Jiang, L. Y.; Bai, H. T.; Liu, L. B.; Lv, F. T.; Ren, X. Q.; Wang, S. *Angew. Chem., Int. Ed.* **2019**, *58*, 10660−10665.

(11) Wu, C. F.; Bull, B.; Szymanski, C.; Christensen, K.; McNeill, J. *ACS Nano* **2008**, *2*, 2415−2423.

(12) Wu, C. F.; Schneider, T.; Zeigler, M.; Yu, J. B.; Schiro, P. G.; Burnham, D. R.; McNeill, J. D.; Chiu, D. T. *J. Am. Chem. Soc.* **2010**, *132*, 15410−15417.

(13) Feng, Y. Q.; Dai, C. H.; Lei, J. P.; Ju, H. X.; Cheng, Y. Q. *Anal. Chem.* **2016**, *88*, 845−850.

(14) Feng, Y. Q.; Sun, F.; Wang, N. N.; Lei, J. P.; Ju, H. X. *Anal. Chem.* **2017**, *89*, 7659−7666.

(15) Wu, T. T.; Cao, Y. W.; Liu, Q.; Wu, X. H.; Shang, Y. X.; Piao, J. F.; Li, Y. J.; Dong, Y. C.; Liu, D. S.; Wang, H. Y.; Liu, J. B.; Ding, B. Q. *J. Am. Chem. Soc.* **2022**, *144*, 6575−6582.

(16) Fu, R.; Xianyu, Y. *Small* **2023**, 2300057.

(17) Hu, T.; Ke, X. X.; Li, W.; Lin, Y.; Liang, A. J.; Ou, Y. J.; Chen, C. X. *Adv. Sci.* **2023**, *10*, 2204689.

(18) Chen, J. S.; Ma, E.; Harrington, L. B.; Da Costa, M.; Tian, X.; Palefsky, J. M.; Doudna, J. A. *Science* **2018**, *360*, 436−439.

(19) Gong, S. H.; Wang, X.; Zhou, P.; Pan, W.; Li, N.; Tang, B. *Anal. Chem.* **2022**, *94*, 15839−15846.

(20) Strecker, J.; Demircioglu, F. E.; Li, D.; Faure, G.; Wilkinson, M. E.; Gootenberg, J. S.; Abudayyeh, O. O.; Nishimasu, H.; Macrae, R. K.; Zhang, F. *Science* **2022**, *378*, 874−881.

(21) Dai, Y. F.; Somoza, R. A.; Wang, L.; Welter, J. F.; Li, Y.; Caplan, A. I.; Liu, C. C. *Angew. Chem., Int. Ed.* **2019**, *58*, 17399−17405.

(22) Xiong, Y.; Zhang, J. J.; Yang, Z. L.; Mou, Q. B.; Ma, Y.; Xiong, Y. H.; Lu, Y. *J. Am. Chem. Soc.* **2020**, *142*, 207−213.

(23) Choi, J. H.; Lim, J.; Shin, M.; Paek, S. H.; Choi, J. W. *Nano Lett.* **2021**, *21*, 693−699.

(24) Zeng, R. J.; Wang, W. J.; Chen, M. M.; Wan, Q.; Wang, C. C.; Knopp, D.; Tang, D. P. *Nano Energy* **2021**, *82*, 105711.

(25) Lin, S. J.; Lin, Y. Z.; Wu, J.; Li, G. M.; Wu, X. T.; Luo, N. N.; Li, W. T.; Zhu, C. L.; Liu, R.; Xu, Q. Q.; Xia, Q. f.; Ju, H. X. *Sens. Actuators B: Chem.* **2023**, *379*, 133204.

(26) Gong, H. X.; Wu, Y. L.; Zeng, R. J.; Zeng, Y. Y.; Liu, X. L.; Tang, D. T. *Chem. Commun.* **2021**, *57*, 8977−8980.

(27) Liu, P. F.; Zhao, K. R.; Liu, Z. J.; Wang, L.; Ye, S. Y.; Liang, G. X. *Biosens. Bioelectron.* **2021**, *176*, 112954.

(28) Zhou, T.; Huang, R.; Huang, M. Q.; Shen, J. J.; Shan, Y. Y.; Xing, D. *Adv. Sci.* **2020**, *7*, 1903661.

(29) Zhang, J.; Gryczynski, Z.; Lakowicz, J. R. *Chem. Phys. Lett.* **2004**, *393*, 483−487.

(30) Bessel, P.; Niebur, A.; Kranz, D.; Lauth, J.; Dorfs, D. *Small* **2023**, *19*, 2206379.

(31) de Barros, H. R.; Garcia, I.; Kuttner, C.; Zeballos, N.; Camargo, P. H. C.; de Torresi, S. I. C.; Lopez-Gallego, F.; Liz-Marzan, L. M. *ACS Catal.* **2021**, *11*, 414−423.

(32) Langhammer, C.; Yuan, Z.; Zoric, I.; Kasemo, B. *Nano Lett.* **2006**, *6*, 833−838.

(33) Xiong, H. W.; Huang, Z. P.; Lin, Q. Y.; Yang, B.; Yan, F.; Liu, B. H.; Chen, H.; Kong, J. L. *Anal. Chem.* **2022**, *94*, 837−846.

(34) Li, K.; Li, Q. L.; Song, L.; Wang, D. Q.; Yin, R. T. *Cancer* **2019**, *125*, 1030−1037.

(35) He, Y. H.; Liu, Y. H.; Cheng, L. J.; Yang, Y. Y.; Qiu, B.; Guo, L. H.; Wang, Y.; Lin, Z. Y.; Hong, G. L. *ACS Appl. Mater. Interfaces.* **2021**, *13*, 298−305.

(36) Liu, Y. J.; Zhang, H. D.; Li, B. X.; Liu, J. W.; Jiang, D. C.; Liu, B. H.; Sojic, N. *J. Am. Chem. Soc.* **2021**, *143*, 17910−17914.
(37) Li, M. X.; Feng, Q. M.; Zhou, Z.; Zhao, W.; Xu, J. J.; Chen, H. Y. *Anal. Chem.* **2018**, *90*, 1340−1347.
(38) Wei, Y.; Zhang, Y. C.; Pan, J. H.; Chen, T.; Xing, X.; Zhang, W. H.; Lu, Z. D. *Angew. Chem., Int. Ed.* **2023**, *62*, e202214103.
(39) Kuo, C. T.; Thompson, A. M.; Gallina, M. E.; Ye, F.; Johnson, E. S.; Sun, W.; Zhao, M.; Yu, J.; Wu, I. C.; Fujimoto, B.; DuFort, C. C.; Carlson, M. A.; Hingorani, S. R.; Paguirigan, A. L.; Radich, J. P.; Chiu, D. T. *Nat. Commun.* **2016**, *7*, 11468.
(40) Wu, C. F.; Hansen, S. J.; Hou, Q.; Yu, J. B.; Zeigler, M.; Jin, Y. H.; Burnham, D. R.; McNeill, J. D.; Olson, J. M.; Chiu, D. T. *Angew. Chem., Int. Ed.* **2011**, *50*, 3430−3434.
(41) Kong, L. Q.; Li, H.; Zhang, X. L.; Zhuo, Y.; Chai, Y. Q.; Yuan, R. *Anal. Chem.* **2022**, *94*, 5167−5172.
(42) Cheng, H.; Li, W.; Duan, S. D.; Peng, J. X.; Liu, J. Q.; Ma, W. J.; Wang, H. Z.; He, X. X.; Wang, K. M. *Anal. Chem.* **2019**, *91*, 10672−10678.
(43) Kachwala, M. J.; Smith, C. W.; Nandu, N.; Yigit, M. V. *Anal. Chem.* **2021**, *93*, 1934−1938.
(44) Guo, Y. Z.; Liu, J. L.; Chen, Y. F.; Chai, Y. Q.; Li, Z. H.; Yuan, R. *Anal. Chem.* **2022**, *94*, 7601−7608.
(45) Miao, W. J. *Chem. Rev.* **2008**, *108*, 2506−2553.
(46) Cai, Z. X.; Li, F. M.; Xu, W.; Xia, S. J.; Zeng, J. B.; He, S. G.; Chen, X. *Nano Res.* **2018**, *11*, 1447−1455.
(47) Tan, X.; Zhang, B.; Zou, G. Z. *J. Am. Chem. Soc.* **2017**, *139*, 8772−8776.
(48) Feng, Y. Q.; Wang, N. N.; Ju, H. X. *Anal. Chem.* **2018**, *90*, 1202−1208.

https://doi.org/10.1021/acs.analchem.3c01521
Anal. Chem. 2023, 95, 7396−7402